

Hydromagnetic dynamos at the low Ekman and magnetic Prandtl numbers

Ján ŠIMKANIN

Institute of Geophysics, Academy of Sciences of the Czech Republic,
Boční II/1401, 141 31 Prague, Czech Republic;
e-mail: jano@ig.cas.cz

Abstract: Hydromagnetic dynamos are numerically investigated at low Prandtl, Ekman and magnetic Prandtl numbers using the PARODY dynamo code. In all the investigated cases, the generated magnetic fields are dominantly-dipolar. Convection is small-scale and columnar, while the magnetic field maintains its large-scale structure. In this study the generated magnetic field never becomes weak in the polar regions, neither at large magnetic Prandtl numbers (when the magnetic diffusion is weak), nor at low magnetic Prandtl numbers (when the magnetic diffusion is strong), which is a completely different situation to that observed in previous studies. As magnetic fields never become weak in the polar regions, then the magnetic field is always regenerated in the tangent cylinder. At both values of the magnetic Prandtl number, strong polar magnetic upwellings and weaker equatorial upwellings are observed. An occurrence of polar magnetic upwellings is coupled with a regeneration of magnetic fields inside the tangent cylinder and then with a not weakened intensity of magnetic fields in the polar regions. These new results indicate that inertia and viscosity are probably negligible at low Ekman numbers.

Key words: Hydromagnetic dynamo, Prandtl number, Magnetic Prandtl number, Inertial forces

1. Introduction

According to present knowledge, the Earth's magnetic field is generated by a self-sustained homogeneous dynamo operating in the liquid part of the Earth's iron core. The theory of hydromagnetic dynamo is able to describe the origin, spatial and temporal evolution of the geomagnetic field and the conditions, which must be satisfied for the dynamo's action (*Roberts and Glatzmaier, 2000; Glatzmaier, 2005; Christensen and Wicht, 2007; Kaiser, 2009; Eltayeb and Rahman, 2013*). In the Earth's core, buoyancy is the fundamental source of (magneto)convection and a hydromagnetic dynamo.

The basic sources of buoyancy are the complicated processes going on in the Earth's fluid interior, for example, a thermal or/and chemical homogenization, gravitational differentiation, solidification processes acting on the inner core boundary, etc. (Jones, 2000; Trümper et al., 2012). The developed dynamo models are mostly based on thermal magnetoconvection for a compressible or incompressible fluid and thermohaline magnetoconvection (Roberts and Glatzmaier, 2000; Christensen and Wicht, 2007). It was assumed that a dynamo could not be precessionally or tidally driven. These models were linear, thus the kinetic energy of fluid motions strongly dissipated in the boundary layers, leading to a malfunctioning dynamo. However, reflecting non-linear terms (the full 3D dynamo problem), numerical simulations showed that precessionally driven dynamos do exist and can provide dipole magnetic fields. Similarly, it appears that the tidally driven flows do not markedly dissipate in the boundary layers. Thus, precessionally and tidally driven flows can be a source for a hydromagnetic dynamo (Le Bars et al., 2011).

Since the first 3D self-consistent dynamo simulation performed by Glatzmaier and Roberts, numerical modelling of self-consistent dynamos has made noticeable progress in the last 20 years due to progress in computer technology (Glatzmaier, 2005; Christensen and Wicht, 2007; Takahashi et al., 2008; Sakuraba and Roberts, 2009; Christensen, 2011; Wicht and Tilgner, 2010). Results of numerical simulations are very similar to the observations of the recent geomagnetic field and to the palaeomagnetic research (Roberts and Glatzmaier, 2000; Christensen and Wicht, 2007). However, many geodynamo models are mostly based on the thermal convection, which provides sufficient and a good approximation of the real conditions in the Earth's fluid interior. Thus, the superadiabatic radial temperature gradient between the core-mantle boundary (CMB) and the inner core boundary (ICB) constitutes the main driving force of convection in most dynamo models without the above mentioned complexities. Nevertheless, recent geodynamo models could be based and many of them are already based on thermochemical convection or convection, which is driven by the heat flux from ICB. The current state of numerical dynamo modelling is described very well in Christensen and Wicht (2007); Takahashi et al. (2008); Takahashi and Shimizu (2012); Sakuraba and Roberts (2009); Christensen (2011); Wicht and Tilgner (2010).

Although the numerical results reproduce more and more detailed features of the Earth's magnetic field, which are provided by observations of the recent geomagnetic field and by palaeomagnetic research (*Aubert et al., 2013*), numerical simulations of the geomagnetic field are not able to run in the Earth-like parameter regime because of the considerable spatial resolution that is required. Geodynamo models in the Earth-like parameter regime are still a great challenge (*Glatzmaier, 2005; Christensen and Wicht, 2007; Sakuraba and Roberts, 2009; Wicht and Tilgner, 2010*). Four basic parameters in this paper models are defined after the Eqs. (1)–(4), two Prandtl numbers, Ekman and Rayleigh numbers, P_r , P_m , E , R_a , respectively. The Prandtl number is the only parameter with a geophysical value that can be directly used in dynamo models. For the outer core of the Earth the kinematic viscosity $\nu = 10^{-6} \text{ m}^2\text{s}^{-1}$, the thermal diffusivity $\kappa = 5 \times 10^{-6} \text{ m}^2\text{s}^{-1}$ and the magnetic diffusivity $\eta = 2 \text{ m}^2\text{s}^{-1}$ are expected (*Roberts and Glatzmaier, 2000; Fearn, 2007*). In most numerical simulations scientists set $\nu/\kappa = 1$ (the ratio ν/κ is known as the Prandtl number).

When it is supposed that the geodynamo model is based on thermal convection, then it is necessary to set $\nu/\kappa < 1$ (*Fearn, 2007*), while when the geodynamo model is based on chemical convection, then it is necessary to use $\nu/\kappa > 1$ (*Christensen and Wicht, 2007; Pozzo et al., 2012*). Thus, when the geodynamo model is driven by the thermochemical convection or by the heat flux from the ICB, then it is possible to set $\nu/\kappa = 1$ (as used in many geodynamo models). *Christensen and Wicht (2007)* estimated values of ν/κ for the outer Earth's core from interval 0.1 – 1. Let us remark that recent estimations of the thermal diffusivity are from $\kappa = 1.4 \times 10^{-7} \text{ m}^2\text{s}^{-1}$ to $\kappa = 9.3 \times 10^{-6} \text{ m}^2\text{s}^{-1}$. This leads to ν/κ from interval 0.1 – 7, which agrees with values expected for thermally driven dynamos ($\nu/\kappa < 1$) and for thermochemically driven dynamos ($\nu/\kappa > 1$). Some recent estimations of the magnetic diffusivity are even $\eta = 12 \text{ m}^2\text{s}^{-1}$, which leads to $\nu/\eta = 10^{-5}$. This is greater than 10^{-6} for $\eta = 2 \text{ m}^2\text{s}^{-1}$ (the ratio ν/η is known as the magnetic Prandtl number, P_m). Nevertheless, other recent estimations of the magnetic diffusivity provide values of $\eta \sim 1 \text{ m}^2\text{s}^{-1}$, which gives $P_m = 10^{-6}$. Recent estimations of the thermal and magnetic diffusivities are provided in *Pozzo et al. (2012)* and *Gomi et al. (2013)*. In this study $\nu/\kappa = 0.2$.

Busse and Simitev (2005; 2011) and *Simitev and Busse (2005)* showed that in the case of low Prandtl numbers, dominantly-dipolar dynamos oc-

curred for larger values of P_m . *Sreenivasan and Jones (2006a)* showed that dipolar dynamo breaks down for $P_m = P_r = 0.2$ because the inertia becomes important, and the magnetic field weakens considerably. There is much more activity in the polar regions at $P_r = 0.2$ than at $P_r = 1$ and as fluid motion becomes strong in the polar regions, the magnetic field gets expelled out of polar regions. *Mishra et al. (2013)* concluded that at low magnetic Prandtl number the decrease of magnetic energy, ohmic dissipation and power of the Lorentz force during a reversal is followed by an increase of the power injected by the force driving the flow and an increase of viscous dissipation. This supports results provided in *Šimkanin (2015)* and *Šimkanin and Hejda (2011; 2013)* at low P_m . *Šimkanin and Hejda (2011; 2013)* found that the magnetic field only becomes weak in the polar regions at low Prandtl numbers and when inertia becomes important. This is a basic condition for such a process. However, whether the magnetic field is weak in the polar regions or not also depends on the magnetic Prandtl number. If the magnetic diffusion is small, then the phenomenon of the magnetic field being weak in the polar regions, does not exist. If it is large, it exists because the strong magnetic diffusion significantly weakens the magnetic field inside the tangent cylinder. The magnetic diffusion and inertia seem to act in the same direction in weakening the magnetic field inside the tangent cylinder (*Šimkanin and Hejda, 2011; 2013*). This is similar to the boundary-locked dynamo investigated in *Sreenivasan (2009)*. The thermal winds are balanced with the Coriolis force. Large lateral variations drive strong radial and axial fluid motions near the equatorial plane; these flows in turn generate the helicity required for dynamo action. The generated magnetic fields are preferred outside the tangent cylinder, as in *Šimkanin and Hejda (2011; 2013)*. For the locked dynamo in *Sreenivasan (2009)* the force balance is the same as for the convection-driven dynamo in *Šimkanin and Hejda (2011; 2013)*.

In this paper hydromagnetic dynamos at the low Ekman number and at low as well as at large magnetic Prandtl numbers are investigated. A main problem is whether the magnetic diffusion and inertia act in the same direction to weaken the magnetic field inside the tangent cylinder when the viscosity is small and the magnetic diffusion is large, i.e. whether magnetic fields become weak in the polar regions at Ekman and magnetic Prandtl numbers lower than those used in *Šimkanin and Hejda (2011; 2013)*. The

model and governing equations are presented in Section 2, numerical results are provided in Section 3 and Section 4 is devoted to discussing the results.

2. Governing equations and model

Here dynamo action that is due to thermal convection of an electrically conducting incompressible fluid in the Boussinesq approximation, in an unstably stratified spherical shell ($r_i < r < r_o$) rotating with angular velocity Ω is considered. The evolution of the magnetic field \mathbf{B} , the velocity \mathbf{V} and the temperature T are described by the following system of dimensionless equations:

$$\frac{\partial \mathbf{B}}{\partial t} = \nabla \times (\mathbf{V} \times \mathbf{B}) + \frac{1}{P_m} \nabla^2 \mathbf{B}, \quad (1)$$

$$\begin{aligned} E \left(\frac{\partial \mathbf{V}}{\partial t} + (\mathbf{V} \cdot \nabla) \mathbf{V} - \nabla^2 \mathbf{V} \right) + 2\mathbf{1}_z \times \mathbf{V} + \nabla P = \\ = R_a \frac{\mathbf{r}}{r_o} T + \frac{1}{P_m} (\nabla \times \mathbf{B}) \times \mathbf{B}, \end{aligned} \quad (2)$$

$$\frac{\partial T}{\partial t} + (\mathbf{V} \cdot \nabla) T = \frac{1}{P_r} \nabla^2 T, \quad (3)$$

$$\nabla \cdot \mathbf{V} = 0, \quad \nabla \cdot \mathbf{B} = 0. \quad (4)$$

The shell gap $L = r_o - r_i$ is the typical length scale, which makes the dimensionless outer core radius $r_o = 1$; the inner core radius r_i is, similar to that of the Earth, equal to 0.35. (r, θ, φ) is the spherical system of coordinates, $\mathbf{1}_z$ is the unit vector. Time, t , is measured in the unit of L^2/ν , velocity, \mathbf{V} , in ν/L , magnetic induction, \mathbf{B} , in $(\rho\mu\eta\Omega)^{1/2}$, superadiabatic temperature, T , in ΔT , and pressure, P , in $\rho\nu^2/L^2$. The dimensionless parameters appearing in Eqs. (1)–(4) are the Prandtl number, $P_r = \nu/\kappa$, the magnetic Prandtl number, $P_m = \nu/\eta$, the Ekman number, $E = \nu/\Omega L^2$ and the modified Rayleigh number $R_a = \alpha g_0 \Delta T L / \nu \Omega$; where κ is the thermal diffusivity, ν is the kinematic viscosity, μ is the magnetic permeability, η is the magnetic diffusivity, ρ is the density, α is the coefficient of thermal expansion, ΔT is the drop of temperature through the shell and g_0 is the

gravity acceleration at $r = r_o$.

Eqs. (1)–(4) are closed by the non-penetrating and no-slip boundary conditions for the velocity field at the rigid surfaces and fixed temperature boundary conditions (the constant temperature $T_i = 1$ and $T_o = 0$ at the inner and outer boundaries of the shell, respectively). The outer boundary is electrically insulating (the magnetic field on this boundary matches with the appropriate potential field in the exterior which implies no external sources of the field), while the inner boundary is electrically conducting (electric conductivity of the outer and inner core is considered to be the same).

3. Numerical results

Eqs. (1)–(4) are solved using the PARODY dynamo code (*Dormy, 1997; Dormy et al., 1998; Aubert et al., 2008; Raynaud and Dormy, 2013*). The code solves the non-dimensional equations in Boussinesq approximation for time-dependent thermal convection in a rotating spherical shell filled with an electrically conducting fluid. PARODY is a semi-spectral code. It uses spherical harmonics decomposition in the lateral and azimuthal directions and a second-order finite differencing scheme in the radial direction, which makes it suitable for parallel computation on distributed memory clusters (*Dormy, 1997; Dormy et al., 1998; Aubert et al., 2008; Raynaud and Dormy, 2013*). As usual, toroidal-poloidal decomposition for velocity and magnetic field is applied. The time integration uses the implicit second-order Crank-Nicolson scheme. Parallelization is carried out using the message-passing interface (MPI). To present the results, DMFI (Dynamical Magnetic Field lines Imaging) visualization is used (*Aubert et al., 2008*). The DMFI algorithm relies on 15 floating anchor points seeded inside the fluid shell. The anchor points are not used as terminations of field lines. The field lines are rendered as tubes with a thickness which is proportional to the local magnetic energy \mathbf{B}^2 . Such a representation naturally depicts the most energetic field lines in the fluid interior and, thus, assigns no visual impact to lines which carry little magnetic energy (*Aubert et al., 2008*). The computations were performed in the Jülich Supercomputing Centre on the Supercomputer JUROPA and the visualizations on the NEMO cluster (SGI) at the Institute

of Geophysics, Academy of Sciences of CR, Prague.

At $P_r = 0.2$ the characteristic viscous diffusion time is five times greater than the characteristic thermal diffusion time ($\tau_\nu = 5\tau_\kappa$); which means that thermal diffusion processes dominate over viscous ones. Computations started from zero initial velocity and a strong dipole-dominated field with $B \sim \mathcal{O}(1)$, and were performed for $P_r = 0.2$. $P_m = 0.1, 0.05$ ($P_{m_{\min}} \simeq 0.01$) and $R_a = 30000$. $P_{m_{\min}}$ is the minimal value of the magnetic Prandtl number at which dipolar dynamos exist. *Christensen and Aubert (2006)* showed that the minimal value of the magnetic Prandtl number at which dipolar dynamos exist varies with the Ekman number as $P_{m_{\min}} \simeq 450E^{3/4}$. This relation was confirmed for $P_r = 0.2$ and $P_m \leq 1$ in *Šimkanin and Hejda (2013)*. The ratio of the Rayleigh number, R_a , to the critical Rayleigh number (the onset of convection), R_{ac} , is 3.1. The spatial resolution was set to $896 \times 432 \times 864$ ($N_r \times N_\theta \times N_\varphi$), where N_r, N_θ, N_φ are the numbers of grid points in the appropriate directions r, θ, φ , respectively. The time integration was performed up to $t = 3.5$ (3.5 time units) for each run. The spatial resolution is quite high, which leads to a small time step, as the spatial resolution and the time step are bounded by the Courant-Friedrichs-Lewy condition for a convergence of solution. Consequently, using these parameters, the time step has to be small, which makes computations pretty time-consuming and then they were performed only up to $t = 3.5$. The cases $P_m < 0.01$ were tested, too. However, for $P_m < 0.01$ and this value of R_a no working dynamos have been found because the magnetic diffusion is too strong to sustain any dynamo. This result confirms the findings of *Christensen and Aubert (2006)*. Thus, the relation between $P_{m_{\min}}$ and E is also valid at $E = 10^{-6}$ and $P_r = 0.2$. Let us briefly comment the efficiency of numerical code and parallelization. Results displayed good convergence and the PARODY code revealed an acceleration, when increase of the number of processors in factor n caused increase of simulations in factor $N > n$ because of the more efficient use of the cash memory. This acceleration, speed-up ($S(P)$), is defined as a ratio of computing time necessary for one processor, $T(1)$, to computing time necessary for P processors, $T(P)$, namely $S(P) = T(1)/T(P)$. $S(P)$ increased with increase of P up to $P = 1500$, when a plateau was obtained (fortunately, the value of P , for which $S(P)$ begins to decrease, has not been reached). Consequently, computations were performed at $P = 1500$.

Dependences of the mean kinetic energy, E_k , the mean magnetic energy, E_m , the ratio of the Rossby number at given P_m to the Rossby number at $P_m = 0.1$, $R_o(P_m)/R_o(P_m = 0.1)$, the magnetic Reynolds number, R_m , and the ratio of the Rossby number to the Elsasser number, R_o/Λ , on the value of the magnetic Prandtl number, P_m , at the Rayleigh number $R_a = 30000$ and the Ekman number $E = 10^{-6}$ are given in Table 1. The mean kinetic energy, E_k , and the mean magnetic energy, E_m , are defined similarly as in *Christensen et al. (2001)*. R_o is defined as $R_o = V/L\Omega$, R_m as $R_m = P_m R_o/E$ and Λ as $\Lambda = B^2/\rho\mu\eta\Omega$. For the given value of R_a , the mean kinetic energy increases with the decrease of P_m , while the mean magnetic energy increases with the increase of P_m , which is caused by stronger magnetic diffusion for lower values of P_m . For the same reason the value of R_m at $P_m = 0.1$ is greater than at $P_m = 0.05$. The values of R_o are comparable, as they are not so different as for larger values of E (*Šimkanin and Hejda, 2011; 2013*). The ratio of the inertial force to the magnetic one (R_o/Λ) is small and, in addition, smaller than for larger values of E (*Šimkanin and Hejda, 2011; 2013*). This could indicate that at $E = 10^{-6}$ and for these parameters the inertia is negligible.

Let us look at magnetic fields and velocities structures. The typical spatial distributions of radial magnetic field components, B_r , at $r = r_o$, are presented in Fig. 1. Both panels are snapshots done at the time $t = 3.5$ (3.5 time units). The magnetic field is dipolar in both the investigated cases but the equatorial symmetry is broken. At $P_m = 0.1$, the generated magnetic field does not become weak in the polar regions ($P_r = 0.2$ but $P_m = 0.1 \gg P_{m_{\min}}$). It is possible to observe fine structures of the magnetic field (small scales are more visible) although the magnetic field maintains

Table 1. Dependences of the mean kinetic energy, E_k , the mean magnetic energy, E_m , the ratio of the Rossby number at given P_m to the Rossby number at $P_m = 0.1$, $R_o(P_m)/R_o(P_m = 0.1)$, the magnetic Reynolds number, R_m , and the ratio of the Rossby number to the Elsasser number, R_o/Λ , on the value of the magnetic Prandtl number, P_m , at the Rayleigh number $R_a = 30000$, the Prandtl number $P_r = 0.2$ and the Ekman number $E = 10^{-6}$.

R_a	P_r	P_m	E_k	E_m	$\frac{R_o(P_m)}{R_o(P_m=0.1)}$	R_m	$\frac{R_o}{\Lambda}$
30000	0.2	0.1	7.6×10^6	4.8×10^7	1.00	390	5.7×10^{-10}
30000	0.2	0.05	8.5×10^6	1.2×10^7	0.96	206	4.9×10^{-9}

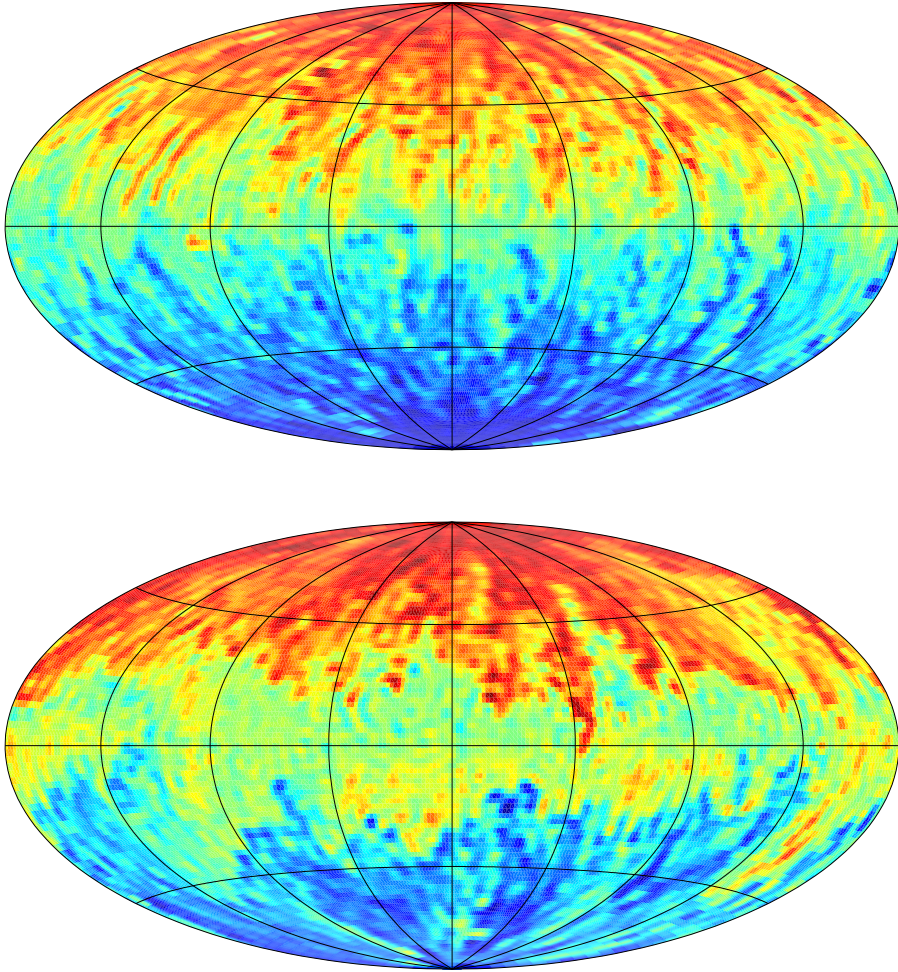


Fig. 1. Spatial distributions (Hammer projections) of radial magnetic field components, B_r , at $r = r_o$ for the Rayleigh number $R_a = 30000$, the Ekman number $E = 10^{-6}$, the Prandtl number $P_r = 0.2$, the magnetic Prandtl number $P_m = 0.1$ (the top row) and 0.05 (the bottom row). Red (blue) colours indicate positive (negative) values. Minimal and maximal values for the first row are $(-27, 27)$ and for the second row $(-19, 19)$. The snapshots are at $t = 3.5$.

its large-scale structure. This case is similar to the case of $P_r = 1$ in *Takahashi et al. (2008)*, so these results support theirs. Decreasing P_m to the value of $P_m = 0.05$ gives a magnetic field, which also does not become weak in the polar regions (similarly to at $P_m = 0.1$, see Fig. 1). The magnetic energy is smaller than in the previous case of $P_m = 0.1$, and the magnetic field weakens but the dynamo remains still dipolar (see Fig. 1). The magnetic diffusion is much stronger than at the previous value of P_m , because $P_m = 0.05$ occurs close to the $P_{m\min}$. The influence of inertial forces in this case is similar to the previous case $P_m = 0.1$ (see Table 1). This leads to a completely different behaviour at values $P_m \simeq P_{m\min}$ than observed at $E = 10^{-5}$ and $E = 10^{-4}$ in *Šimkanin and Hejda (2013)*, and at $E = 10^{-3}$ in *Šimkanin and Hejda (2011)*. In previous cases the magnetic fields always became weak in polar regions at $P_r = 0.2$ and for values $P_m \simeq P_{m\min}$. At $E = 10^{-6}$ it is not so (see Fig. 1).

As in *Šimkanin and Hejda (2013)*, let us focus on the tangent cylinder. Equatorial sections of the radial magnetic field components, B_r , axisymmetrical meridional sections of the poloidal magnetic field components, B_P , the toroidal magnetic field components, B_T , (at $P_m = 0.1, 0.05$) and equatorial sections of the the radial velocity field components, V_r , axisymmetrical meridional sections of the poloidal velocity field components, V_P , and of the toroidal velocity field components, V_T , (at $P_m = 0.1, 0.05$) are presented in Fig. 2. All the panels are snapshots done at $t = 3.5$. The red (blue) colours indicate positive (negative) values. At $P_m = 0.1$, the magnetic field raises larger upwelling that creates in turn stronger magnetic fields inside the tangent cylinder and this growth is weakly limited by magnetic diffusion (see Fig. 2). This is the effect firstly described in *Sreenivasan and Jones (2006b)*, namely inside the tangent cylinder, in the region of the polar vortices, thermal winds are strongly modified by magnetic winds due to Lorentz force. Thus, the magnetic field is strong enough to initiate the polar magnetic upwelling which stabilizes the stronger magnetic field in the polar region (see Figs. 1–2). The magnetic upwelling as well as other structures described in the framework of the DMFI is provided in the next paragraph. As shown in *Šimkanin and Hejda (2013)*, the absence of this effect is responsible for the weak magnetic field in the polar regions at low Prandtl numbers. At $P_m = 0.05$, the situation is the same as at $P_m = 0.1$, meaning that the magnetic field is regenerated in the tangent cylinder at both $P_m = 0.1$ and

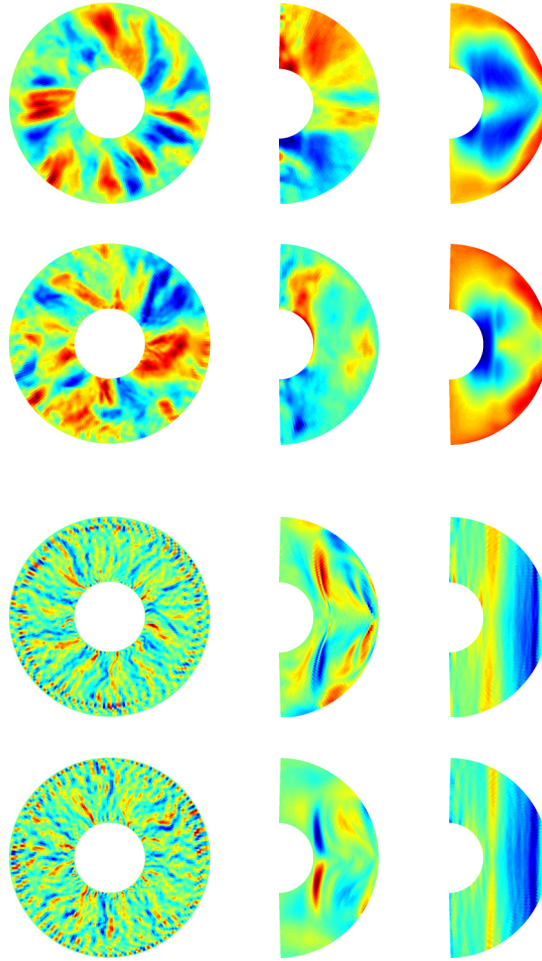


Fig. 2. Equatorial sections of the radial components, axisymmetrical meridional sections of the poloidal components and axisymmetrical meridional sections of the toroidal components (from left to right) of the magnetic field, \mathbf{B} , at the magnetic Prandtl number $P_m = 0.1$, the magnetic field, \mathbf{B} , at the magnetic Prandtl number $P_m = 0.05$, the velocity field, \mathbf{V} , at the magnetic Prandtl number $P_m = 0.1$ and the velocity field, \mathbf{V} , at the magnetic Prandtl number $P_m = 0.05$ (from top to bottom); for the Rayleigh number $R_a = 30000$, the Ekman number $E = 10^{-6}$ and the Prandtl number $P_r = 0.2$. Red (blue) colours indicate positive (negative) values. Minimal and maximal values for the first row are $(-27, 27)$, $(-22, 22)$, $(-24, 24)$, for the second row $(-19, 19)$, $(-15, 15)$, $(-9.96, 9.96)$, for the third row $(-17, 17)$, $(-12, 12)$, $(-16, 16)$ and for fourth row $(-18, 18)$, $(-13, 13)$, $(-17, 17)$. The snapshots are at $t = 3.5$.

$P_m = 0.05$, and it is strong enough to initiate the above mentioned effect of *Sreenivasan and Jones (2006b)*. Consequently, it does not become weak in the polar regions even though the magnetic field is weaker than at $P_m = 0.1$ due to large magnetic diffusion (see Figs. 1–2). At $P_m = 0.05$ there is a little larger upwelling compared to the case $P_m = 0.1$ (see Fig. 2), but it does not constrain from a recovery of magnetic field inside the tangent cylinder. Thus, inertial forces do not play such a significant role as at $E \geq 10^{-5}$ although $P_r = 0.2$ (*Šimkanin and Hejda, 2011; 2013*).

The generated magnetic fields are large-scale at both values of P_m (0.1 and also 0.05, see Fig. 2). Nevertheless, it is possible to observe fine structures of the magnetic field; since at $E = 10^{-6}$ small scales are more visible than at $E = 10^{-5}$ (see *Šimkanin and Hejda, 2013*), although the magnetic field maintains its large-scale structure. Velocity fields are columnar and small-scale at both values of P_m (see Fig. 2). The columnar character of convection is maintained due to this value of R_a ; since the Rayleigh number is approximately three times greater than its critical value, while the small-scale character of convection is given by the low value of the Ekman number. At low Ekman numbers a small-scale columnar convection dominates, while the magnetic field maintains its large-scale structure (see Figs. 2–3). Consequently, as in *Takahashi et al. (2008)* the scales of the flow and magnetic field are separated (see Fig. 3). The scale separation enables hydromagnetic dynamos to maintain the magnetic field at low values of P_m . This explains why $P_{m,\min}$ decreases with decrease of E (*Takahashi et al., 2008; Christensen and Aubert, 2006; Schaeffer and Cardin, 2006*).

In Fig. 2 some sheet-like flows are observed, providing support for the results published in *Takahashi and Shimizu (2012)*. It is not strange, because the sheet-like flows occur irrespective of boundary conditions and driving mode of convection as long as the Ekman number is small enough, while spatial distribution of convection seems to be sensitive to the thermal boundary conditions, strength and morphology of the generated magnetic field (*Takahashi and Shimizu, 2012*). However, this study does not observe a formation of the meandering type d structure at $E = 10^{-6}$, which contrasts with the findings of *Takahashi and Shimizu (2012)*. The convection structures in *Takahashi and Shimizu (2012)* are described in the next paragraphs. This supports the results of *Aubert et al. (2008)* at the high value of E and *Šimkanin and Hejda (2013)* at the same value of E as in *Taka-*

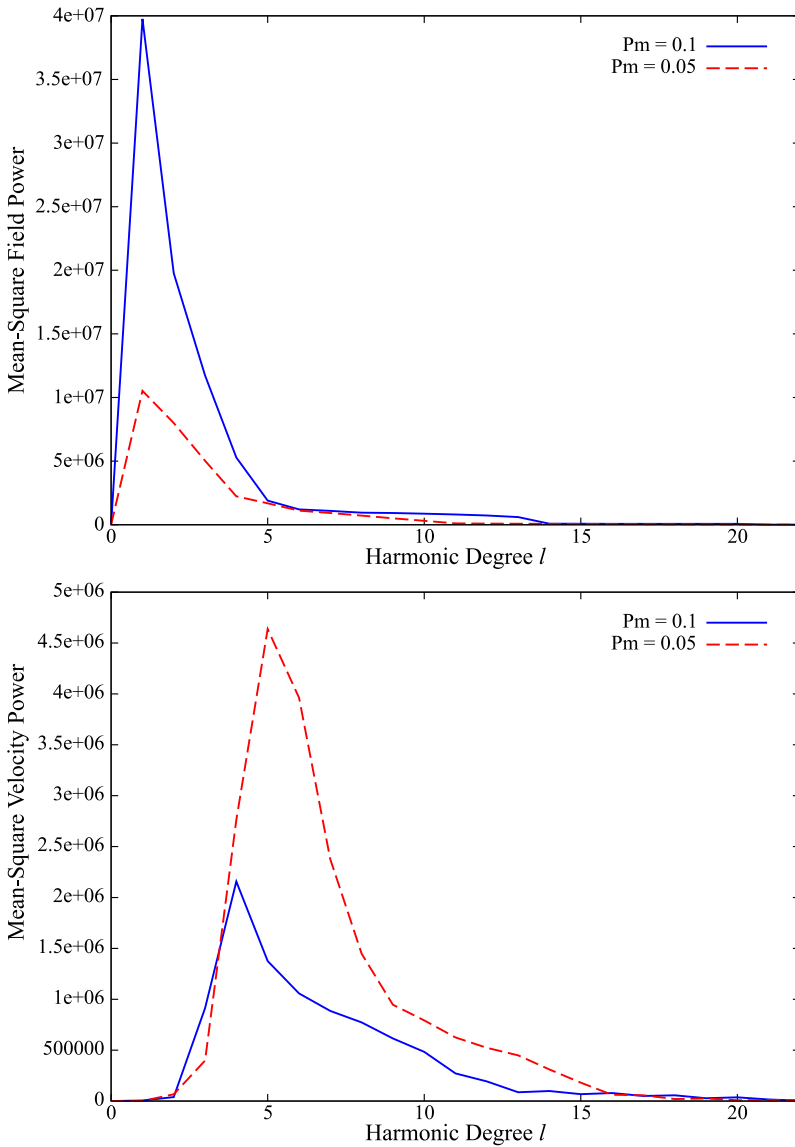


Fig. 3. The mean-square magnetic field power spectrum (the top row) and the mean-square velocity field power spectrum (the bottom row) as a function of harmonic degree l in dependence on the magnetic Prandtl number, P_m , ($P_m = 0.1$ depicted by solid lines and $P_m = 0.05$ depicted by dotted lines).

hashi and Shimizu (2012), because a formation of the meandering type d structure was also not observed in *Aubert et al. (2008)* and *Šimkanin and Hejda (2013)*.

The typical spatial distributions of the magnetic field, \mathbf{B} , as well as other structures related to DMFI are presented in Fig. 4. All the panels are snapshots done at $t = 3.5$. The left-hand panel provides the top (polar) view, the right-hand panel the side view. The ICB and CMB boundaries are colour-coded with the radial magnetic field, B_r . The red (blue) colours indicate outwards (inwards) oriented fields. The field lines are rendered as tubes with a thickness that is proportional to the local magnetic energy \mathbf{B}^2 . The radial magnetic field as seen from the Earth's surface is presented in the upper-right inserts (for more details, see *Aubert et al., 2008*). In both the investigated cases, $P_m = 0.1$ and $P_m = 0.05$, dynamos are dipolar and the generated magnetic fields do not become weak in the polar regions, although the magnetic field at $P_m = 0.05$ is weaker than at $P_m = 0.1$. At both values of P_m it is possible to observe strong polar magnetic upwellings and weaker equatorial magnetic upwellings (see Fig. 4). At $P_m = 0.1$ more equatorial upwellings than at $P_m = 0.05$ are observed. Both cases in Fig. 4 ($P_m = 0.1$ and $P_m = 0.05$) illustrate how the poloidal component of magnetic field is stretched in the azimuthal direction and this process is well described by the magnetic anticyclones. The magnetic anticyclones result from the magnetic field's interaction with axial flow anticyclones (*Aubert et al., 2008*). Strong polar magnetic upwellings are equivalent to the large upwelling that may create strong fields inside the tangent cylinder and then regenerates the magnetic field inside the tangent cylinder (the effect described in *Sreenivasan and Jones, 2006b*). Thus, an occurrence of strong polar magnetic upwellings is coupled with a recovery of magnetic fields inside the tangent cylinder, leading to the strong magnetic field in the polar regions, which means that the magnetic field does not become weak in the polar regions (see Figs. 1–4). Comparing Fig. 4 with the results in *Šimkanin and Hejda (2013)*, strong polar magnetic upwellings are now really equivalent to the large upwelling that may create strong fields inside the tangent cylinder and then regenerates the magnetic field inside the tangent cylinder (*Sreenivasan and Jones, 2006b*), which leads to a strong magnetic field in the polar regions, meaning that the magnetic field does not become weak in the polar regions. However, in *Šimkanin and Hejda (2013)* at $P_m = 0.1$, no polar

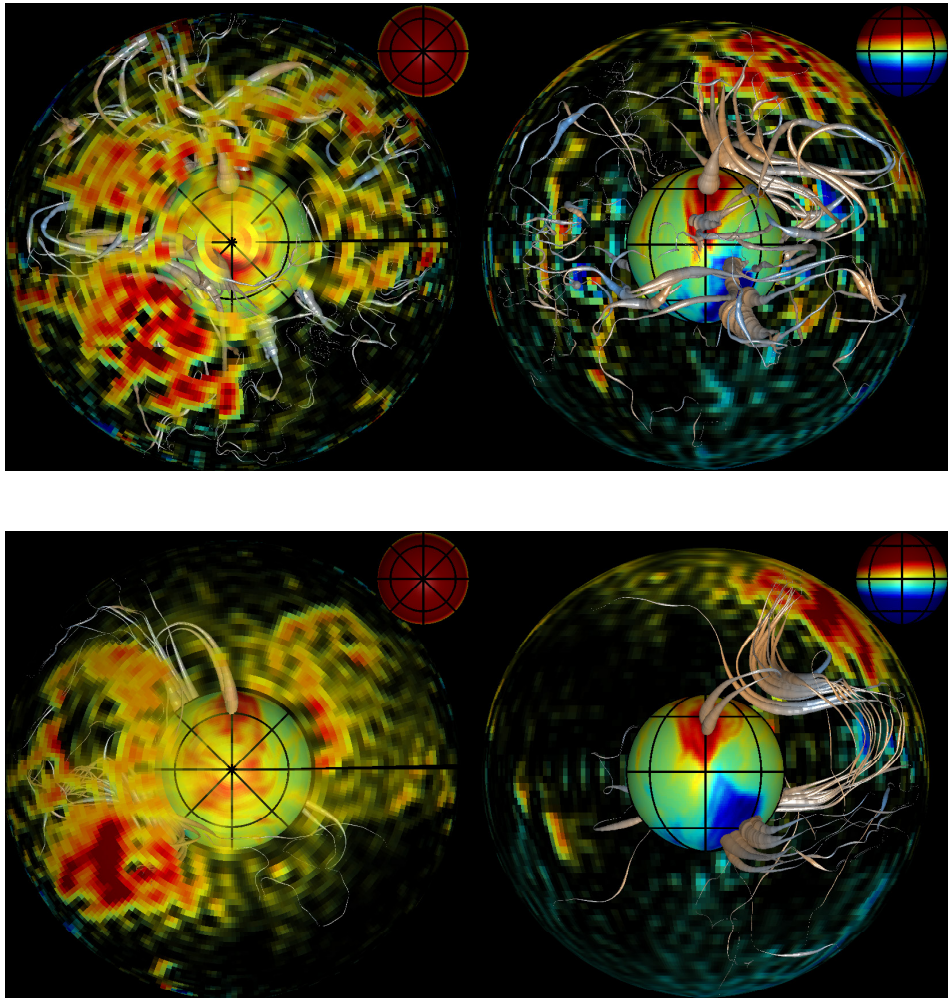


Fig. 4. The spatial distributions of magnetic field \mathbf{B} for the Rayleigh number $R_a = 30000$, the Ekman number $E = 10^{-6}$, the Prandtl number $P_r = 0.2$, the magnetic Prandtl number $P_m = 0.1$ (the top row) and 0.05 (the bottom row). The left-hand panels provide the top (polar) view, the right-hand panels the side view. The ICB and CMB boundaries are colour-coded with the radial magnetic field, B_r . Red (blue) colours indicate outwards (inwards) oriented field. The field lines are rendered as tubes with a thickness that is proportional to the local magnetic energy \mathbf{B}^2 . The radial magnetic field as seen from the Earth's surface is presented in the upper-right inserts. The snapshots are at $t = 3.5$.

magnetic upwellings but only weak equatorial upwellings were observed. Thus, the magnetic field is localized mostly outside the tangent cylinder and is weak inside the tangent cylinder (here, it is not regenerated), which leads to the weak magnetic field in the polar regions, so that the magnetic field becomes weak in the polar regions. Now, it is possible to conclude that an occurrence of polar magnetic upwellings is coupled with magnetic fields inside the tangent cylinder and then with magnetic fields in the polar regions (see Šimkanin and Hejda, 2013 and Fig. 4 in this paper).

At $E = 10^{-6}$, the influence of inertial forces becomes weak and the magnetic diffusion and inertia do not act in the same direction to weaken the magnetic field inside the tangent cylinder. The magnetic diffusion is a predominant factor at this value of E . Consequently, in contrast to the findings of Šimkanin and Hejda (2011; 2013) the effects of inertia are noticeably visible at higher values of E . Thus, these results indicate that at low Ekman numbers the effects of the viscosity and inertia are dynamically negligible compared to the Lorentz, Coriolis and buoyancy forces.

4. Discussion

Numerical modelling of rotating convection and hydromagnetic dynamos showed strong dependence on the Prandtl number and the magnetic Prandtl number (Busse and Simitev, 2005; 2011; Simitev and Busse, 2005; Sreenivasan and Jones, 2006a; 2006b; Brestenský et al., 1998; Šimkanin et al., 2010; Šimkanin and Hejda, 2011; 2013). Results for $E = 10^{-3}$, 10^{-4} and 10^{-5} , presented in Šimkanin and Hejda (2011; 2013), provide the following conclusions. Convection in the case of $P_r = 0.2$ is more supercritical than for $P_r = 1$ at a given value of R_a (the critical Rayleigh number, R_{ac} , decreases with decrease of P_r). Dynamos always remain dipolar for these parameters. Inertia becomes important (the Rossby numbers are large compared to the case $P_r = 1$, when they are small), but its influence on the dynamo action and magnetic field structures is regulated by the magnetic Prandtl number. The phenomenon of the magnetic field being weak in the polar regions, is observed primarily at small values of P_r (Sreenivasan and Jones, 2006b). It is a basic condition but it is necessary to remark here that the weak geomagnetic field near the poles was also observed at $P_r = 1$ in Olson et al. (1999) and Aubert (2005). However, whether the magnetic field is weak in

the polar regions or not also depends on the magnetic Prandtl number. At large values of P_m , the magnetic field raises larger upwelling that in turn creates stronger magnetic fields inside the tangent cylinder. This growth is weakly limited by magnetic diffusion and magnetic fields in the polar regions do not become weak. The small magnetic diffusion eliminates the influence of inertia on the magnetic field structures and dynamo action. This indicates that the so-called MAC balance probably dominates, the inertia could be negligible in the force balance, and does not influence the connection between flow upwellings and magnetic field inside the tangent cylinder (a magnetic influence dominates over inertial one). In this case $R_o/\Lambda \ll 1$ (see Table 2). This is similar to the case when $P_r = 1$. Decreasing P_m weakens the magnetic field inside the tangent cylinder, which leads to the magnetic field becoming weak in the polar regions. For $P_m \simeq P_{m_{\min}}$ the magnetic field significantly weakens (but remains dipolar) and it is significantly weak in the polar regions because of an extremely weak magnetic field inside the tangent cylinder. Here it is necessary to note that *Aubert (2005)* observed hydromagnetic processes at $P_r = 1$, when magnetic fields were pushed out of the tangent cylinder, which led to relatively weak magnetic flux in polar regions. However, it was a case of non-dipolar dynamos in contrast to this case of dipolar dynamos. For $P_m \simeq P_{m_{\min}}$ the inertia can influence the connection between flow upwellings and the magnetic field inside the tangent cylinder, but the magnetic diffusion influence remains the main factor in these processes. Nevertheless, the so-called MAC balance probably does not dominate over the inertia (see Table 2), so that the influence of rotation, viscosity and buoyancy could be more important. *Soderlund et al. (2012)* and *King and Buffett (2013)* proposed the so-called VAC balance. Results indicate that when magnetic fields in the polar regions become significantly weak due to a magnetic field being extremely weak inside the tangent cylinder, then the VAC balance could be preferred to the MAC balance. This is this case for $E = 10^{-3}, 10^{-4}$ and 10^{-5} (*Šimkanin and Hejda, 2011; 2013*). However, results provide only some indications because such conclusions require a detailed force balance analysis, which has been done in *Soderlund et al. (2012)* and *King and Buffett (2013)* but it was not done in *Šimkanin and Hejda (2011; 2013)*. For $P_m < P_{m_{\min}}$ dynamos fail.

At $E = 10^{-6}$ the situation is completely different compared to cases $E = 10^{-5}$, $E = 10^{-4}$ in *Šimkanin and Hejda (2013)* and at $E = 10^{-3}$ in

Šimkanin and Hejda (2011). The magnetic field at $E = 10^{-6}$ in both the investigated cases ($P_m = 0.1, 0.05$) is dipolar and never becomes weak in the polar regions, though $P_r = 0.2$. Neither at large values of P_m (the magnetic diffusion is weak), nor at low values of P_m (the magnetic diffusion is strong). The magnetic field is always regenerated in the tangent cylinder and it is strong enough to initiate the effect described in Sreenivasan and Jones (2006b). Consequently, it does not become weak in the polar regions even though the magnetic field is weak at values $P_m \simeq P_{m_{\min}}$ due to large magnetic diffusion. Thus, the influence of inertial forces becomes weak and the magnetic diffusion and inertia do not act in the same direction in weakening the magnetic field inside the tangent cylinder (see Table 2). Probably, magnetic diffusion is a predominant factor at this value of $E = 10^{-6}$. Then, $R_o/\Lambda \ll 1$ (see Table 2). Consequently, the effects of inertia are noticeably visible at higher values of E , as was observed in Šimkanin and Hejda (2011; 2013). At $E = 10^{-6}$ results indicate that at low Ekman numbers the inertia could be negligible, so that the so-called MAC balance probably dominates and it is not influenced by the inertia. King and Buffett (2013) showed that the so-called VAC balance proposed in Soderlund et al. (2012) and King and Buffett (2013) is inappropriate at low Ekman numbers and the so-called MAC balance is more appropriate because the influence of Lorentz forces is paramount and the role of viscosity is no longer important. As written before, these results provide only some indications because such conclusions require a detailed force balance analysis, which is not done in this study.

Table 2. Dependences of the ratio of the Rossby number to the Elsasser number, R_o/Λ , on the value of the Ekman number, E , and the magnetic Prandtl number, P_m . Y/N means if magnetic fields weaken in the polar regions (Yes/No).

E	P_m	R_o/Λ	Magnetic fields weaken in the polar regions
10^{-3}	3	2.4×10^{-6}	Y
10^{-4}	1	6.9×10^{-8}	N
10^{-4}	0.5	1.9×10^{-7}	Y
10^{-5}	0.5	7.8×10^{-9}	N
10^{-5}	0.1	9.3×10^{-8}	Y
10^{-6}	0.1	5.7×10^{-10}	N
10^{-6}	0.05	4.8×10^{-9}	N

Aubert et al. (2008) defined magnetic upwellings (MU) as energetic field lines generated within buoyancy-driven flow upwellings and they observed them as the most remarkable structures highlighted by DMFI sequences. The existence of MU has previously been suspected through the appearance of tangent cylinder CMB flux patches closely related to helical flow upwelling plumes (*Sreenivasan and Jones, 2006b*). A polar magnetic upwelling is created by thermal and magnetic wind-driven plumes, which reside within the tangent cylinder. The converging flow beneath upwellings concentrates the ICB magnetic flux patches into intense spots seeding the magnetic field growth. Stretching and advection inside the upwellings subsequently amplify the magnetic field bundle which rises in the direction of the rotation axis. Magnetic upwellings inside the tangent cylinder rise within helical flow plumes which are not colinear but parallel to the rotation axis. Equatorial magnetic upwellings are created close to the equatorial part of the ICB, where the concentrated magnetic flux patches get near to the quasi-geostrophic columnar flow upwellings residing outside the tangent cylinder. The mechanism for their generation is largely the same as that of polar magnetic upwellings. However, they are not associated with helical flow plumes since the ambient vorticity field is not stretched by cylindrical radial motion. Equatorial upwellings, therefore, lack the magnetic flux expulsion mechanism seen with polar upwellings, and have little to no observable signature at the CMB. Results show that strong polar magnetic upwellings are equivalent to the large upwelling that may create and then regenerate strong fields inside the tangent cylinder as was described in *Sreenivasan and Jones (2006b)*. An effect described in *Sreenivasan and Jones (2006b)* showed a connection between flow upwellings and magnetic field inside the tangent cylinder. Strong magnetic fields seem to lead to larger upwelling that may then in turn create stronger fields until this growth is limited by diffusion. For low values of P_m , the magnetic field could be too weak to initiate the effect and there would be little field created inside the tangent cylinder (*Sreenivasan and Jones, 2006b*). At large values of P_m the magnetic diffusion is weak and strong polar magnetic upwellings are observed, but equatorial magnetic upwellings are weaker than polar ones (see Fig. 4 in this paper and *Šimkanin and Hejda, 2013*). Thus, strong polar magnetic upwellings occur together with a recovery of magnetic fields inside the tangent cylinder, which leads to a strong magnetic field in the polar regions. The

magnetic field does not become weak in the polar regions (see Fig. 4 in this paper and Šimkanin and Hejda, 2013). At low values of P_m and $E \geq 10^{-5}$ the magnetic diffusion is strong and no polar magnetic upwellings are observed, but rather only weak equatorial upwellings (Šimkanin and Hejda, 2013). The magnetic field is localized mostly outside the tangent cylinder and is weak inside the tangent cylinder (here, it is not regenerated), which leads to a weak magnetic field in the polar regions. Thus, the magnetic field becomes weak in the polar regions (Šimkanin and Hejda, 2013). However, at large and low values of P_m and Ekman numbers ($E \leq 10^{-6}$) strong polar magnetic upwellings and equatorial magnetic upwellings are observed and they are weaker than polar ones, which leads to a strong magnetic field in the polar regions, so that the magnetic field does not become weak in the polar regions.

Takahashi and Shimizu (2012) investigated the hydromagnetic dynamo, which was driven by volumetric internal heating or secular cooling, at $E = 10^{-5}$, $P_r = 1$, $P_m = 2$ and $R_a = 3 \times 10^7$ (2.6 times the R_{ac}). This dynamo is characterized by the approximate magnetostrophic (MAC) balance, where the effects of the viscosity and inertia are dynamically negligible compared to the Lorentz, Coriolis and buoyancy forces. Their convection structures are characterized by the co-existence of localized thin sheet-like plumes and large-scale retrograde azimuthal flows. Such a mixed structure is a result of the strong azimuthal magnetic field at low latitudes near the outer boundary associated with a retrograde flows (type a). The mixed style of convection generates a strong magnetic field with typical structures (Takahashi and Shimizu, 2012). The type a and radial and axial fields in low to mid latitude associated with the downwelling plumes (type b) accompany the current loop structure, which is formed by stretching of the magnetic lines along the direction of local magnetic field by acceleration of the flow. Axial and azimuthal fields in mid latitude near the rim of the tangent cylinder (type c) are formed by twist and stretch of the field lines by the shear flow (Takahashi and Shimizu (2012)). The meandering type d is observed temporally. It is made from the type a magnetic field and intense sheet plumes. The main loop part of the structure is seemingly similar to that associated with anti-cyclonic vortex (Aubert et al., 2008). On the other hand, Aubert et al. (2008) investigated hydromagnetic dynamos at a much higher value of E . They set $E = 10^{-2}$. This study does not observe a

formation of the meandering type d structure at $E = 10^{-6}$, which contrasts with the findings of *Takahashi and Shimizu (2012)*. This supports the results of *Aubert et al. (2008)* at the high value of E and *Šimkanin and Hejda (2013)* at the same value of E as in *Takahashi and Shimizu (2012)*, because a formation of the meandering type d structure was not observed in *Aubert et al. (2008)* and *Šimkanin and Hejda (2013)*, too. A different driving force of convection may play a role. *Takahashi and Shimizu (2012)* assumed the top forcing, while *Aubert et al. (2008)* employed bottom forcing (the same as in this study). Since flows near the outer boundary tend to be active compared with the deep part in the top forcing case, such flows could generate the type d structure from the type a magnetic field near the outer boundary. As the meandering type d structure is not observed and the bottom forcing is employed, this study supports the results of *Aubert et al. (2008)*. However, some sheet-like flows are/were observed also in this investigation, which supports the findings of *Takahashi and Shimizu (2012)*. This is not strange because the sheet-like flows occur irrespective of boundary conditions and driving mode of convection as long as the Ekman number is small enough, while spatial distribution of convection seems to be sensitive to the thermal boundary conditions, strength and morphology of the generated magnetic field *Takahashi and Shimizu (2012)*. The small-scale columnar convection dominates, while the magnetic field maintains its large-scale structure. Scales of the flow and magnetic field are separated (see Fig. 3), which enables hydromagnetic dynamos to maintain the magnetic field at low values of P_m . *Schaeffer and Cardin (2006)* studied a kinematic dynamo at very small Ekman and magnetic Prandtl numbers. They supposed a 2D quasi-geostrophy model for the flow and 3D model for the magnetic field, and concluded that a dynamo action could exist at low P_m due to scale separation. The same conclusion is provided in *Takahashi and Shimizu (2012)* for the 3D full dynamo. *Brandenburg (2009)* investigated large-scale dynamos driven by helical forcing. He concluded that in the absence of helicity, there is only small-scale dynamo action, which is driven by the dynamics at the smallest possible scale, namely the resistive scale.

The preliminary results of a study at $E = 10^{-7}$ and $P_r = 0.2$ support these conclusions. The occurrence of polar magnetic upwellings is associated with regeneration of magnetic fields inside the tangent cylinder and

then probably with the intensity of magnetic fields in the polar regions.

Acknowledgements. This research has been supported by the Ministry of Education, Youth and Sports through project No. LG13042 and the Jülich Supercomputing Centre through project No. 99000539. I would like to thank Emmanuel Dormy and Julien Aubert for the PARODY dynamo code and the DMFI visualization tools, the Jülich Supercomputing Centre for CPU time on the Supercomputer JUROPA and the Institute of Geophysics, Academy of Sciences of the Czech Republic, Prague for CPU time on the NEMO cluster (SGI).

References

- Aubert J., 2005: Steady zonal flows in spherical shell dynamos. *J. Fluid Mech.*, **542**, 53–67.
- Aubert J., Aurnou J., Wicht J., 2008: The magnetic structure of convection-driven numerical dynamos. *Geophys. J. Int.*, **172**, 945–956.
- Aubert J., Finlay C. C., Fournier A., 2013: Bottom-up control of geomagnetic secular variation by the Earth’s inner core. *Nature*, **502**, 219–223, doi: 10.1038/nature12574.
- Brandenburg A., 2009: Large-scale dynamos at low magnetic Prandtl numbers. *ApJ*, **697**, 1206–1213, doi: 10.1088/0004-637X/697/2/1206.
- Brestenský J., Ševčík S., Šimkanin J. 1998: Magnetoconvection in dependence on Roberts number. *Studia Geophys. Geod.*, **42**, 280–288.
- Busse F. H., Simitev R., 2005: Convection in rotating spherical fluid shells and its dynamo states. In: Soward A. M., Jones C. A., Hughes D. W., Weiss N. O. (Eds.), *Fluid Dynamics and Dynamos in Astrophysics and Geophysics*, **359–392**, CRC Press, New York, USA.
- Busse F. H., Simitev R., 2011: Remarks on some typical assumptions in dynamo theory. *Geophys. Astrophys. Fluid Dyn.*, **105**, 234–247.
- Christensen U. R., Aubert J., Cardin P., Dormy E., Gibbons S., Glatzmaier G. A., Grote E., Honkura Y., Jones C., Kono M., Matsushima M., Sakuraba A., Takahashi F., Tilgner A., Wicht J., Zhang K., 2001: A numerical dynamo benchmark. *Phys. Earth Planet. Inter.*, **128**, 25–34.
- Christensen U. R., Aubert J., 2006: Scaling properties of convection-driven dynamos in rotating spherical shells and application to planetary magnetic fields. *Geophys. J. Int.*, **166**, 97–114.
- Christensen U. R., Wicht J., 2007: Numerical dynamo simulations. In: Kono M. (Ed.), *Volume 8 – Core Dynamics*, 245–282, Schubert G. (Ed.-in-Chief), *Treatise on Geophysics*, Elsevier, Amsterdam, The Netherlands.
- Christensen U. R., 2011: Geodynamo models: Tools for understanding properties of Earth’s magnetic field. *Phys. Earth Planet. Int.*, **187**, 157–169.

- Dormy E., 1997: Numerical modeling of the geodynamo (Modélisation numérique de la dynamo terrestre). PhD Thesis, Institut de Physique du Globe de Paris, (in French).
- Dormy E., Cardin P., Jault D., 1998: MHD flow in a slightly differentially rotating spherical shell, with conducting inner core, in a dipolar magnetic field. *Earth Planet. Sci. Lett.*, **160**, (1–2), 15–30.
- Eltayeb I. A., Rahman M. M., 2013: Model III: Benard convection in the presence of horizontal magnetic field and rotation. *Phys. Earth Planet. Int.*, **221**, 38–59.
- Fearn D. R., 2007: 4.1. The Earth and its magnetic field. In: Soward A. M., Dormy E. (Eds.), *Mathematical Aspects of Natural Dynamos*, 201–209, CRC Press, New York, USA.
- Glatzmaier G. A., 2005: Planetary and stellar dynamos: challenges for next generation models. In: Soward A. M., Jones C. A., Hughes D. W., Weiss N. O. (Eds.), *Fluid Dynamics and Dynamos in Astrophysics and Geophysics*, 331–357, CRC Press, New York, USA.
- Gomi H., Ohta K., Hirose K., Labrosse S., Caracas R., Verstraete M. J., Hernlund J. W., 2013: The high conductivity of iron and thermal evolution of the Earth's core. *Phys. Earth Planet. Inter.*, **224**, 88–103.
- Jones C. A., 2000: Convection-driven geodynamo models. *Phil. Trans. R. Soc. Lond. A*, **358**, 873–897, doi: 10.1098/rsta.2000.0565.
- Kaiser R., 2009: On purely toroidal dynamo magnetic fields caused by conductivity variations. *Geophys. Astrophys. Fluid Dyn.*, **103**, 6, 503–513.
- King E. M., Buffett B. A., 2013: Flow speeds and length scales in geodynamo models: The role of viscosity. *Earth Planet. Sci. Lett.*, **371–372**, 156–162.
- Le Bars M., Wiczkorek M. A., Karatekin Ö., Cébron D., Laneuville M., 2011: An impact-driven dynamo for the early Moon. *Nature*, **479**, 215–218, doi: 10.1038/nature10565.
- Mishra P., Gissinger C., Dormy E., Fauve S., 2013: Energy transfers during dynamo reversals. *EPL*, **104**, 6, 69002-p1–69002-p6, doi: 10.1209/0295-5075/104/69002.
- Olson P., Christensen U. R., Glatzmaier G. A., 1999: Numerical modeling of the geodynamo: mechanisms of field generation and equilibration. *J. Geophys. Res.*, **104**, 10, 383–404.
- Pozzo M., Davies C., Gubbins D., Alfè D., 2012: Thermal and electrical conductivity of iron at Earth's core conditions. *Nature*, **485**, 355–358, doi: 10.1038/nature11031.
- Raynaud R., Dormy E., 2013: Intermittency in spherical Couette dynamos. *Phys. Rev. E*, **87**, 033011.
- Roberts P. H., Glatzmaier G. A., 2000: Geodynamo theory and simulations. *Rev. Mod. Phys.*, **72**, 4, 1081–1123.
- Sakuraba A., Roberts P. H., 2009: Generation of a strong magnetic field using uniform heat flux at the surface of the core. *Nature Geosci.*, **2**, 802–805.
- Schaeffer N., Cardin P., 2006: Quasi-geostrophic kinematic dynamos at low magnetic Prandtl number. *Earth Planet. Sci. Lett.*, **245**, 595–604.
- Simitev R., Busse F. H., 2005: Prandtl-number dependence of convection-driven dynamos in rotating spherical fluid shells. *J. Fluid Mech.*, **532**, 365–388.

- Šimkanin J., Hejda P., Saxonbergová-Jankovičová D., 2010: Convection in rotating non-uniformly stratified spherical fluid shells in dependence on Ekman and Prandtl numbers. *Phys. Earth Planet. Inter.*, **178**, 39–47.
- Šimkanin J., Hejda P., 2011: Hydromagnetic dynamos in rotating spherical fluid shells in dependence on the Prandtl number and stratification. *Geophys. J. Int.*, **185**, 637–646.
- Šimkanin J., Hejda P., 2013: Magnetic fields generated by hydromagnetic dynamos at the low Prandtl number in dependence on the Ekman and magnetic Prandtl numbers. *Phys. Earth Planet. Int.*, **217**, 22–30, doi: 10.1016/j.pepi.2012.11.002.
- Šimkanin J., 2015: Polarity reversals in dependence on the Prandtl number and density stratification. *Studia Geophys. Geod.*, **59**, 137–158, doi: 10.1007/s11200-014-0724-6.
- Soderlund K. M., King E. M., Aurnou J. M., 2012: The influence of magnetic fields in planetary dynamo models. *Earth Planet. Sci. Lett.*, **333–334**, 9–20.
- Sreenivasan B., Jones C. A., 2006a: The role of inertia in the evolution of spherical dynamos. *Geophys. J. Int.*, **164**, 467–476.
- Sreenivasan B., Jones, C. A., 2006b: Azimuthal winds, convection and dynamo action in the polar regions of planetary cores. *Geophys. Astrophys. Fluid Dyn.*, **100**, 319–339.
- Sreenivasan B., 2009: On dynamo action produced by boundary thermal coupling. *Phys. Earth Planet. Int.*, **177**, 130–138.
- Takahashi F., Matsushima M., Honkura Y., 2008: Scale variability in convection-driven MHD dynamos at low Ekman number. *Phys. Earth Planet. Int.*, **167**, 168–178.
- Takahashi F., Shimizu H., 2012: A detailed analysis of a dynamo mechanism in a rapidly rotating spherical shell. *J. Fluid Mech.*, **701**, 228–250.
- Trümper T., Breuer M., Hansen U., 2012: Numerical study on double-diffusive convection in the Earth's core. *Phys. Earth Planet. Int.*, **194**, 55–63.
- Wicht J., Tilgner A., 2010: Theory and modeling of planetary dynamos. *Space Sci. Rev.*, **152**, 501–542.